Catalysis Communications 57 (2014) 78–82

Contents lists available at ScienceDirect

Catalysis Communications

journal homepage: www.elsevier.com/locate/catcom

Short Communication

Dendrimer-stabilized bimetallic Pd/Au nanoparticles: Preparation, characterization and application to vinyl acetate synthesis

Martin Kuhn [a,*], Janine Jeschke [b], Steffen Schulze [c], Michael Hietschold [c], Heinrich Lang [b], Thomas Schwarz [a]

[a] Faculty of Natural Science, Institute of Chemistry, Technical Chemistry, Technische Universität Chemnitz, 09107 Chemnitz, Germany
[b] Faculty of Natural Science, Institute of Chemistry, Inorganic Chemistry, Technische Universität Chemnitz, 09107 Chemnitz, Germany
[c] Faculty of Natural Science, Institute of Physics, Solid Surfaces Analysis & Electron Microscopy Laboratory, Technische Universität Chemnitz, 09107 Chemnitz, Germany

ARTICLE INFO

Article history:
Received 28 March 2014
Received in revised form 31 July 2014
Accepted 5 August 2014
Available online 14 August 2014

Keywords:
Dendrimer-stabilized Pd/Au nanoparticles
Vinyl acetate synthesis
Silica supported Pd/Au catalyst
TEM

ABSTRACT

The preparation, characterization and a novel application to vinyl acetate synthesis of dendrimer-stabilized Pd/Au nanoparticles are described. The nanoparticles were synthesized by co-precipitation of aqueous Pd^{2+}/Au^{3+} salt solutions with hydrazine in the presence of (poly)amidoamine (PAMAM)-based dendrimers functionalized with terminal ethylene glycol ethers. Characterization by transmission electron microscopy and UV–vis spectroscopy confirmed that alloyed Pd/Au nanoparticles with a mean diameter of 6.0 (±1.2) to 10.4 (±1.7) nm were formed. After nanoparticle immobilization onto a silica support and thermal dendrimer removal, the resulting materials are high active catalysts in ethylene acetoxylation to vinyl acetate monomer with a productivity of 2.1 $kg_{VAM}\ kg_{cat}^{-1}\ h^{-1}$.

1. Introduction

Bimetallic nanoparticles are of significant scientific and technological interest due to their unique chemical, optical and electronic properties [1]. Particularly with regard to their catalytic performance they often provide better activity, selectivity or stability than their monometallic counterparts [2]. One of the most studied bimetallic materials is the Pd/Au system, as it exhibits a high activity towards a huge number of useful chemical reactions such as CO oxidation [3], oxidation of primary alcohols to aldehydes [4], hydrogenation of hydrocarbons [5], electrochemical reactions [6] and acetoxylation of ethylene to vinyl acetate [7].

Vinyl acetate monomer (VAM) is an essential basic chemical with a global output of more than 6 million tons in 2011 [8]. It is primarily required for the production of a variety of polymers like polyvinyl acetate, polyvinyl alcohol and vinyl acetate copolymers [9]. Currently, more than 80% of annual VAM production is obtained via vapor-phase acetoxylation of ethylene over Pd-based catalysts [9].

Industrially, different processes were developed but most plants operate according to the Bayer–Hoechst process established in 1968 [10,11]. A typical egg-shell catalyst for VAM synthesis consists of 0.2–4.0 wt.% Pd, 0.1–2.0 wt.% Au and 1–10 wt.% KOAc supported on SiO_2 or Al_2O_3 with a productivity of 2.1 $kg_{VAM}\ kg_{cat}^{-1}\ h^{-1}$ [12]. Nakamura and Yasui first described the promotional effect of KOAc [13,14]. The key to bimetallic Pd/Au catalysts that are made up of reactive Pd and unreactive Au is the distribution of the metals on the alloyed surface to create active ensembles for VAM synthesis. The active ensemble has been suggested to comprise two, isolated Pd atoms, also known as the ensemble-effect [15–17]. The main role of Au is to break contiguous Pd atom ensembles at the surface. Provine and co-workers found out that the resulting isolated Pd monomers were more active for acetoxylation of ethylene to vinyl acetate than contiguous Pd sites [18]. Moreover, the isolated Pd monomer surface sites suppress the combustion of ethylene [19] and the deactivation by formation of Pd carbides on the catalyst surface [15].

The catalytic properties of bimetallic Pd/Au nanoparticles mainly depend not only on their size and shape but also on their structure (alloy, core–shell) and surface composition [20,21]. There are two possibilities to prepare bimetallic nanoparticles from metal salts: co-reduction and successive reduction [22]. The simultaneous reduction of two metal salts is the most simple preparation method and can lead to alloy or core–shell structures depending on reaction conditions. Successive reduction normally produces core–shell structured bimetallic nanoparticles [23].

Herein, we report the synthesis and characterization of dendrimer-stabilized bimetallic Pd/Au nanoparticles prepared via co-reduction of $Pd(NO_3)_2$ and $H[AuCl_4]$, respectively, in the presence of (poly)amidoamine (PAMAM)-based dendrimers with end-grafted ethylene glycol ether moieties (Scheme 1). Dendrimers, with their highly branched, monodisperse, radial-symmetric structure, are well suited as stabilizing component for metal nanoparticles [24–27]. Compared to other applied dendrimers, the functionalized PAMAM species **1** and **2** provide a high number of donor functionalities per gram, which are still well

* Corresponding author. Tel.: +49 6151 16 3766; fax: +49 6151 16 4788.
E-mail address: kuhn@ct.chemie.tu-darmstadt.de (M. Kuhn).

http://dx.doi.org/10.1016/j.catcom.2014.08.009
1566-7367/

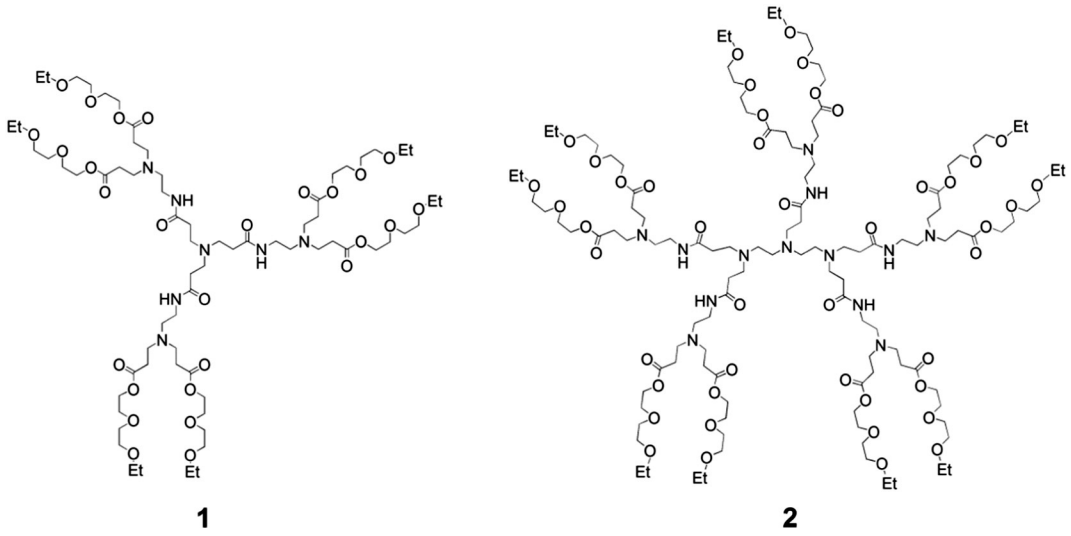

Scheme 1. Oligo(ethylene glycol)-functionalized PAMAM-based dendrimers **1** and **2**.

characterizable (e.g., by NMR techniques) and are easily accessible in a three-step synthesis methodology [25,26,28,29]. Systems **1** and **2** were used as metal precursor for the preparation of silica supported Pd/Au catalysts. The resulting catalysts were tested in acetoxylation of ethylene to vinyl acetate.

2. Experimental

2.1. Preparation procedure for Pd/Au nanoparticles

The oligo(ethylene glycol)-terminated PAMAM dendrimers **1** and **2** were synthesized according to previously published procedures [25,26]. Dendrimer-stabilized Pd/Au nanoparticles (NP) were prepared by the chemical co-precipitation method (Scheme 2). To receive the appropriate metallodendrimer, the Pd^{2+} and Au^{3+} ions were coordinated at the dendrimer donor functionalities. Therefore, a solution of [$Pd(NO_3)_2$···2 H_2O] (18.7 mg, 0.07 mmol) and H[$AuCl_4$···3 H_2O] (11.8 mg, 0.03 mmol) in H_2O (100 mL) was prepared. This Pd^{2+}/Au^{3+} solution (2 mL, 1 mM) was mixed with a solution of dendrimer **1** or **2** in H_2O (2 mL) in different ratios (dendrimer: $[Pd^{2+}/Au^{3+}] = 1:1$ (1 mM:1 mM), 1:10 (0.1 mM:1 mM), 1:50 (0.02 mM:1 mM), 1:100 (0.01 mM:1 mM), 1:150 (6.67 μM:1 mM) or 1:200 (5 μM:1 mM)). The resulting orange–brown mixture was stirred for 10 min followed by the reduction of the respective Pd^{2+}/Au^{3+} ions with hydrazine hydrate (100%, 40 μL), whereby the solution color changed to black. The Pd/Au NP were characterized with TEM (Philips CM 20, 200 kV, 300–1000 particles for determination of the average particle size) and UV–vis spectroscopy (Genesys 6 spectrophotometer Thermo Electron Corporation, 25 °C).

2.2. Catalyst preparation

The appropriate Pd/Au catalysts (2.5 wt.% nominal Pd and 1.99 wt.% Au loading) were synthesized by the co-precipitation of palladium(II) nitrate and tetrachloroaurate(III) in the presence of PAMAM-based dendrimers **1** and **2** onto silica as supporting material. Reduction occurred by liquid phase reduction with hydrazine.

To dendrimer **1** (10.0 mg, 6.72 μmol) or dendrimer **2** (14.4 mg, 6.72 μmol) (Scheme 1) dissolved in H_2O (10 mL) a solution of [$Pd(NO_3)_2$···2 H_2O] (125 mg, 470 μmol) in H_2O (20 mL) was added dropwise. Subsequently, a solution of H[$AuCl_4$···3 H_2O] (79.3 mg, 201 μmol) in H_2O (10 mL) was added. The resulting orange–brown colored mixture was stirred for 2 h at ambient temperature followed by the addition of silica (2.0 g). After 18 h of stirring the respective Pd^{2+} and Au^{3+} ions were reduced by dropwise adding of hydrazine monohydrate (1.0 mL, 13 mmol) under vigorous stirring, while the mixture color immediately changed to black.

After aging the mixture for additional 2 h, H_2O was removed by rotary evaporator. The resulting material was homogenized with a mortar and dried at 110 °C for 12 h before it was calcined in air (350 °C, 3 h). Finally, the catalyst was washed with H_2O (700 mL), dried over night at 50 °C and homogenized again.

The catalysts were characterized with TGA/DSC (Mettler-Toledo TGA/DSC 1100 system with an UMX1 balance, nitrogen/oxygen 2:1, 30 °C to 600 °C, 10 K min^{-1}) and via inductively coupled plasma optical

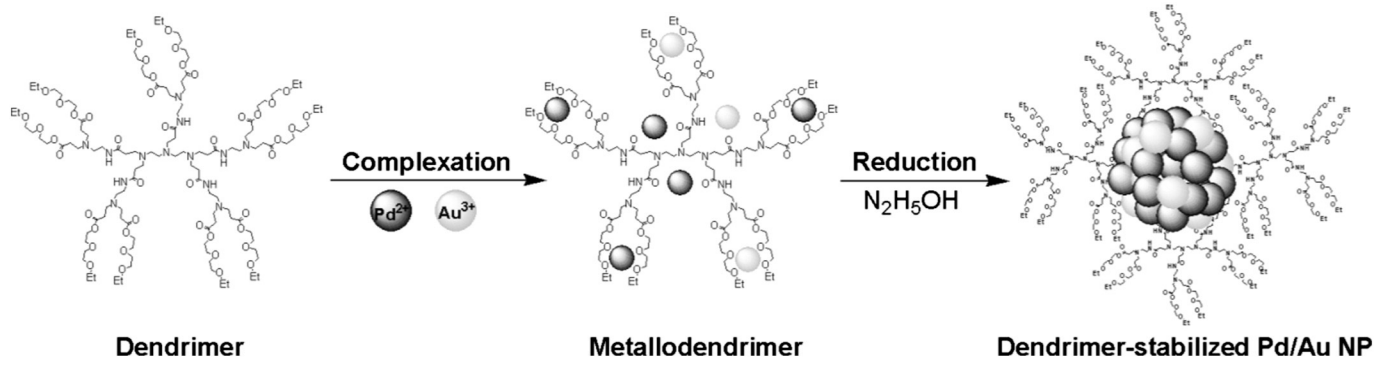

Scheme 2. Schematic illustration of the formation of bimetallic Pd/Au nanoparticles.

emission spectrometry (ICP-OES) with a Vista-MPX (Varian). X-ray powder diffraction patterns of all samples were obtained by STOE-STAD-IP diffractometer using Cu-$K_{\alpha 1}$-radiation (1.5405 Å, 40 kV, 40 mA) and a Ge(111)-monochromator.

2.3. Fixed bed reactor and the reaction conditions

All experiments for catalyst performance in VAM synthesis were carried out in a continuous flow system. The reactor consisting of a 0.25 inch inner diameter and 10.25 inch length stainless steel tube filled with 0.4 g catalyst and 8.0 g SiC was impregnated with 4.0 wt.% KOAc. The feed mixture contains 50.0 vol.% ethylene, 6.5 vol.% oxygen, 18.0 vol.% acetic acid, as well as 1.5 vol.% cyclohexane as internal standard and nitrogen as diluting agent. Acetic acid and cyclohexane were vaporized in the presence of ethylene and nitrogen in an evaporator at 190 °C. All tubes were heated to 160 °C to prevent a condensation of the reactants and products. The gas hourly space velocity (GHSV) was varied from 15 $Nm^3\ kg_{cat}^{-1}\ h^{-1}$ to 20 $Nm^3\ kg_{cat}^{-1}\ h^{-1}$ and the reactor temperature from 150 °C to 170 °C at an excess pressure of 8 bar. The mixture leaving the reactor was analyzed by gas chromatography (CP-3800, Varian, FID). After condensing volatile compounds at −9 °C, the amounts of oxygen (Oxynos 100, Rosemount) as well as CO and CO_2 (Binos 1001, Rosemount) were determined continuously in the exhaust gas. All experiments were performed for 5 h at each temperature and GHSV, respectively. Furthermore a pre-run period of 5 h at 150 °C and 20 $Nm^3\ kg_{cat}^{-1}\ h^{-1}$ was upstreamed.

3. Results and discussion

To confirm a bimetallic structure for the Pd/Au nanoparticles UV–vis absorbance spectroscopy was used. Therefore the spectra of bimetallic nanoparticles containing various metal compositions (0:100, 30:70, 50:50, 70:30 and 100:0 molar ratios of $[Pd(NO_3)_2]$:H$[AuCl_4]$) were compared with the spectra of respective monometallic particle dispersions (Fig. 1). The molar ratio of stabilizer **2** to metal salts was maintained constant at 1:100. Fig. 1a shows a series of UV–vis spectra for different ratios of Pd and Au monometallic nanoparticles. With all samples that contain monometallic Au nanoparticles a characteristic surface plasma adsorption at approximately 540 nm was observed [30]. The adsorption peak increased with decreasing Pd/Au ratio. The sample of pure monometallic Pd nanoparticles revealed as expected no adsorption between 350 and 800 nm [30]. The UV–vis spectra for the bimetallic Pd/Au nanoparticles, as illustrated in Fig. 1b, exhibit a different absorption behavior but no surface plasma adsorption is found. These investigations indicate that the dispersions of nanoparticles prepared by co-precipitation of Pd^{2+} and Au^{3+} do not contain monometallic Au particles, but nanoparticles with bimetallic structure. This is consistent with spectra reported for bimetallic Pd/Au nanoparticles [31,32].

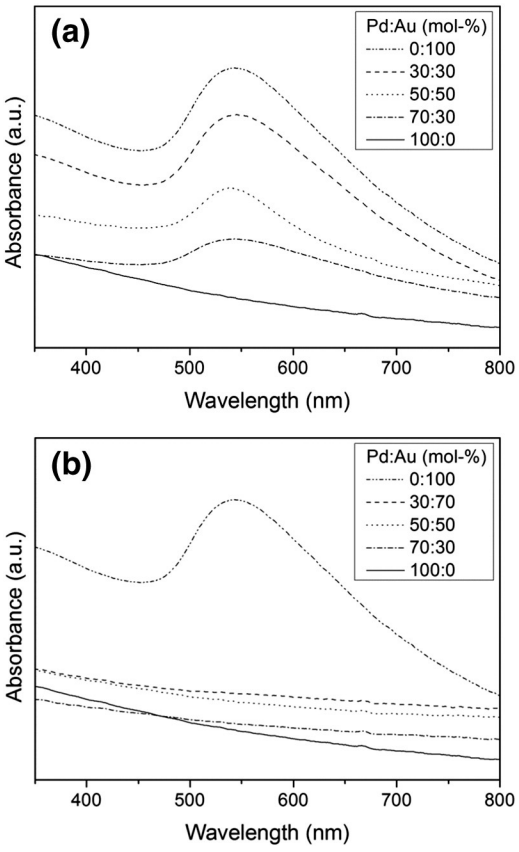

Fig. 1. UV–vis spectra of (a) monometallic **2**-Pd and **2**-Au nanoparticles and (b) bimetallic **2**-Pd/Au nanoparticles with various molar metal ratios and constant dendrimer-to-metal ratio of 1:100.

TEM images were used to determine the individual particle size, size distribution and morphology of the appropriate dendrimer-stabilized Pd/Au nanoparticles (Fig. 2). In all cases almost regular spherical shaped nanoparticles were formed. Moreover, the alloyed structure of the received nanoparticles could be confirmed by electron diffraction patterns and XRPD (for more information see supplementary data S1). The electron diffraction ring pattern affiliated by TEM verifies a face centered cubic (fcc) structure and exhibits a lattice constant of 4.0 Å, which lies between the lattice constants of pure Au (4.08 Å) and Pd (3.89 Å) [33].

In general, Pd/Au nanoparticles with a particle size between 6.0 (±1.2) and 10.4 (±1.7) nm were obtained. The size of the gained dendrimer-stabilized Pd/Au nanoparticles thereby depends on the type of dendrimer and the correspondent dendrimer-to-metal ratio. From Fig. 2 it can be seen that with a constant molar dendrimer-to-metal ratio of 1:100 and a constant Pd:Au ratio of 70:30 the **2**-Pd/Au nanoparticles (Ø 8.1 ± 1.5 nm) are smaller than the **1**-Pd/Au nanoparticles (Ø 9.6 ± 1.4 nm). Obviously, dendrimer **2** is a better stabilizer because of its higher number of terminal ethylene glycol moieties, preventing further particle growth.

Table 1 shows that the particle size can also be controlled by molar dendrimer-to-metal ratio. As expected, an increasing stabilizer ratio leads with both dendrimers to decreasing nanoparticle sizes. The morphology of dendrimer-stabilized Pd/Au nanoparticles is not affected by the type of stabilizer or dendrimer-to-metal ratio.

The respective dendrimer-stabilized Pd/Au nanoparticles were used as metal precursors for the preparation of silica-supported Pd/Au catalysts and tested for their productivity in VAM synthesis. Therefore the metallodendrimers were immobilized onto a silica support by liquid phase reduction with hydrazine and calcined. All catalysts were prepared with a constant molar dendrimer to metal ratio of 1:100, a constant Pd:Au ratio of 70:30 and a nominal Pd loading of 2.5 wt.%. The catalyst loadings were determined by ICP-OES. The results approve a complete fixation of the noble metals onto the supporting material (for more information see Supplementary data S2).

The XRPD patterns of the calcined catalysts (Fig. 3) show the expected reflexes of a Pd/Au alloy at 39°, 46° and 67°. Additionally there are reflexes caused by silica (60°, 71°) and by the formation of PdO (34°, 55°) [34]. The crystallite size of the Pd/Au alloy calculated by Scherrer rises with increasing calcination temperature from 5 nm at 300 °C up to 24 nm at 550 °C (for more information see Supplementary data S3). This observation indicates the sintering of single crystallites to larger agglomerated particles at higher temperatures.

Furthermore, Fig. 3 reveals an increase of crystallinity and an adjustment of the Pd/Au reflexes to smaller angles with increasing calcination temperature. This adjustment is caused by the formation of PdO at high temperatures, which exhibits another crystal structure than Pd and Au [35].

Due to economic reasons, in order to receive small crystallite sizes and to inhibit the formation of PdO, a low calcination temperature

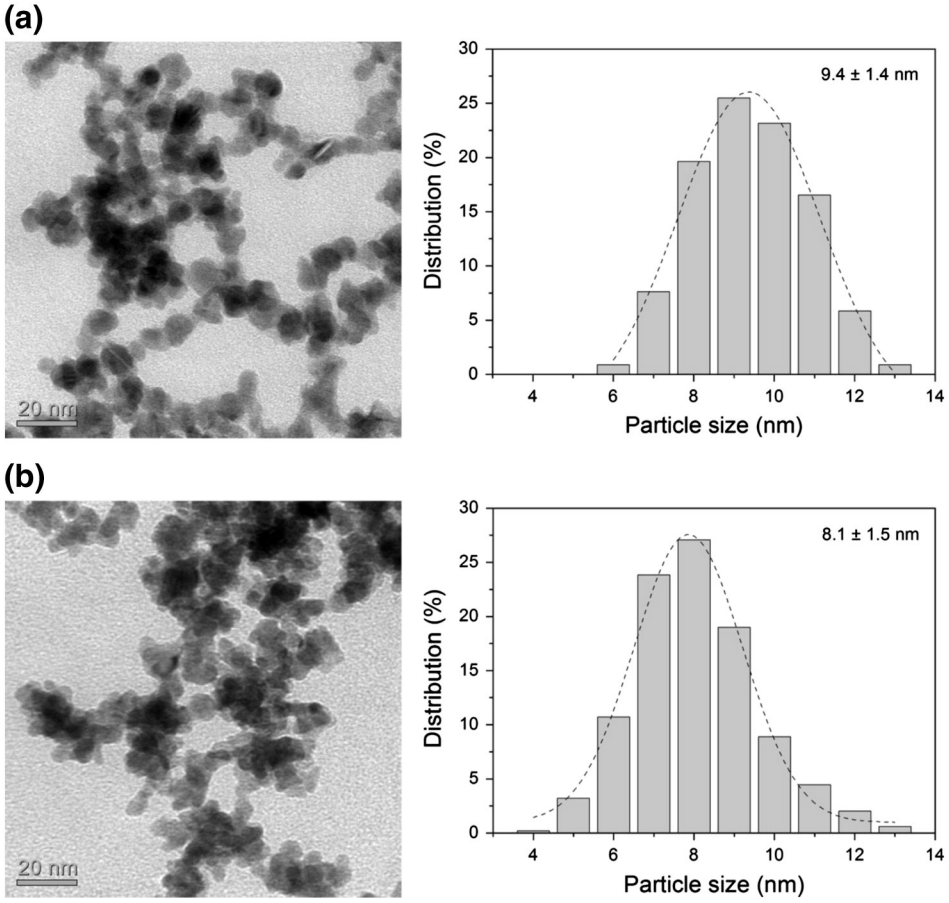

Fig. 2. TEM images and particle size distribution of (a) **1**-Pd/Au nanoparticles and (b) **2**-Pd/Au nanoparticles each with a molar dendrimer-to-metal ratio of 1:100 and constant Pd:Au ratio of 70:30.

should be selected. But crucial to the catalytic performance of the resulting catalysts is also a preferably complete removal of the stabilizer (for more information see Supplementary data S4). Therefore a calcination temperature of 350 °C was chosen.

Chemical reaction engineering studies of the VAM catalysts were performed in a continuous flow system. The results for the catalytic runs in VAM synthesis are shown in Fig. 4. In general the productivity rises from 150 °C and 15 $Nm^3\ kg_{cat}^{-1}\ h^{-1}$ to 170 °C and 20 $Nm^3\ kg_{cat}^{-1}\ h^{-1}$ with a maximum in productivity of 2.1 $kg_{VAM}\ kg_{cat}^{-1}\ h^{-1}$ for catalyst **1**_hydrazine. Moreover, the results in Fig. 4 exhibit a better productivity for the catalysts prepared with dendrimer **1** in comparison to **2**. Catalysts prepared by **1** exhibit higher oxygen activities and selectivities at all reaction conditions than catalysts prepared by **2** (Table 2). This is contrary to the findings in TEM imaging, which revealed smaller Pd/Au nanoparticles by stabilization with dendrimer **2** and thereby indicates a higher catalytic surface. These results confirm an incomplete removal of the stabilizers by thermal treatment at 350 °C. Due to the larger dendrimeric scaffold of stabilizer **2**, more catalytic active sites are blocked by remaining donor functionalities and consequently inhibit a better catalytic performance. For checking all reported results a carbon mass balance was calculated, which confirmed to 100%.

Table 1
Particle sizes of dendrimer-stabilized Pd/Au nanoparticles with various molar dendrimer-to-metal ratios and constant Pd:Au ratio of 70:30 determined by TEM measurement.

Entry	Molar ratio of dendrimer: Pd/Au (mol%)	Particle size (nm) **1**-Pd/Au	Particle size (nm) **2**-Pd/Au
1	1:10	6.0 ± 1.2	6.5 ± 2.2
2	1:50	7.9 ± 1.5	7.0 ± 1.5
3	1:100	9.4 ± 1.4	8.1 ± 1.5
4	1:150	10.1 ± 1.6	9.4 ± 2.0
5	1:200	10.4 ± 1.7	9.7 ± 1.6

4. Conclusion

Dendrimer-stabilized Pd/Au nanoparticles with varying size between 6.0 (±1.2) and 10.4 (±1.7) nm have been prepared by the chemical co-precipitation method. The size was adjusted by varying the dendrimer-to-metal ratio and the type of dendrimeric scaffold. Generally, reducing the proportion of stabilizer leads to an increase in particle size. Furthermore, dendrimer **2** tends to produce smaller particles because of its larger scaffold and higher number of donor functionalities.

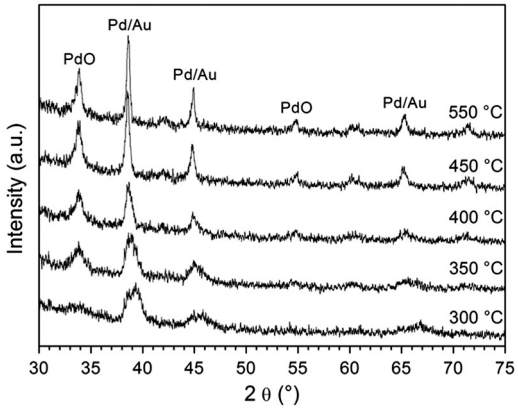

Fig. 3. XRPD patterns of catalyst 1_hydrazine calcined at various temperatures (Pd loading: 5 wt.%, Au loading: 4 wt.%).

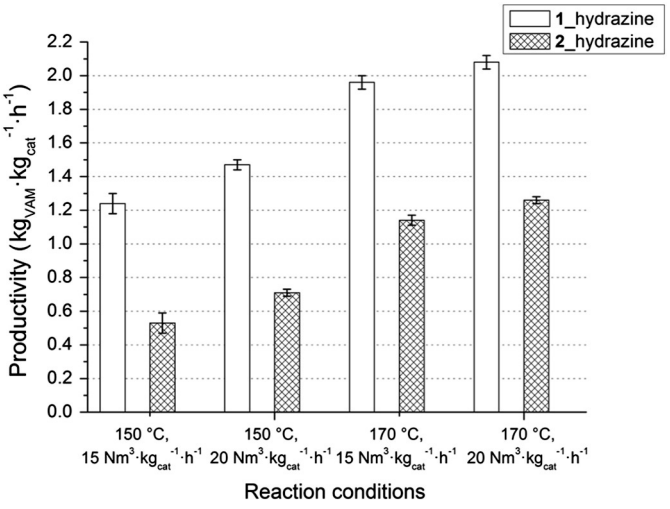

Fig. 4. VAM productivities for Pd/Au catalysts with a nominal Pd loading of 2.5 wt.% for 150 °C, 170 °C and two different GHSVs.

Table 2
Catalytic results for VAM catalysts prepared by immobilization of dendrimer-stabilized Pd/Au nanoparticles, see Section 2.3 for reaction conditions.

Catalyst	ϑ (°C)	GHSV ($Nm^3/(kg_{cat} \cdot h)$)	P_{cat} ($kg_{VAM}/(kg_{cat} \cdot h)$)	X_{O2} (%)	$S_{VAM/O2}$ (%)
1_hydrazine	150	15	1.2	31.2	52.9
		20	1.5	28.7	51.4
	170	15	2.0	48.3	54.1
		20	2.1	38.8	53.7
2_hydrazine	150	15	0.5	20.7	33.9
		20	0.7	22.0	32.3
	170	15	1.1	33.6	45.3
		20	1.3	29.2	43.4

The alloy structure of the Pd/Au nanoparticles was confirmed by UV–vis spectroscopy and TEM imaging.

By immobilizing the dendrimer-stabilized nanoparticles onto a silica support and thermal dendrimer removal, active catalysts for VAM synthesis with a maximum productivity of 2.1 $kg_{VAM}\, kg_{cat}^{-1}\, h^{-1}$ were obtained, which can compete with industrially used catalysts in VAM synthesis [12]. Moreover, the calcination temperature has a crucial influence on the catalyst properties. The higher the calcination temperature, the larger are the resulting Pd/Au crystallites and the more PdO is formed. But a high calcination temperature is required for complete dendrimer removal. The reason for the worse productivity of catalysts prepared with dendrimer **2** is presumably the blocking of active sites due to incomplete dendrimer removal.

Acknowledgement

We gratefully acknowledge Maik Schlesinger (XRPD), Colin Georgi (TGA) and Heike Fingerle (ICP-OES) for the assistance in experimental work. We are grateful to the Fonds der chemischen Industrie for the financial support.

Appendix A. Supplementary data

Supplementary data to this article can be found online at http://dx.doi.org/10.1016/j.catcom.2014.08.009. These data include MOL files and InChiKeys of the most important compounds described in this article.

References

[1] M. Harada, K. Asakura, N. Toshima, J. Phys. Chem. 97 (1993) 5103–5114.
[2] Y. Suo, I.-M. Hsing, Electrochim. Acta 56 (2011) 2174–2183.
[3] L. Guczi, A. Beck, A. Horváth, Z. Koppány, G. Strefler, K. Frey, I. Sajó, O. Geszti, D. Bazin, J. Lynch, J. Mol. Catal. A Chem. 204–205 (2003) 545–552.
[4] D.I. Enache, J.K. Edwards, P. Landon, B. Solsona-Espriu, A.F. Carley, A.A. Herzing, M. Watanabe, C.J. Kiely, D.W. Knight, G.J. Hutchings, Science 311 (2006) 362–365.
[5] A. Sárkany, A. Horváth, A. Beck, Appl. Catal. A 229 (2002) 117–125.
[6] C. Xu, Z. Tian, Z. Chen, S.P. Jiang, Electrochem. Commun. 10 (2008) 246–249.
[7] M. Chen, D.W. Goodman, Chin. J. Catal. 29 (2008) 1178–1186.
[8] G. Mestl, A. Reltzmann, Luft für schnelle Ergebnisse, discover Süd-Chemie, 2012.
[9] G. Roscher, Ullmann's Encyclopedia of Industrial Chemistry, WILEY-VCH Verlag GmbH & Co. KGaA, Weinheim, 2012.
[10] H. Holzrichter, W. Krönig, B. Frenz, Bayer AG, BE 627 888, 1962.
[11] H. Fernholz, H.-J. Schmidt, F. Wunder, Hoechst, DE-AS 1 296 138, 1967.
[12] K. Büker, S. Schirrmeister, B. Langanke, A. Geißelmann, G. Markowz, R. Hausmann, DE102004050585A1, Degussa AG, 40474 Düsseldorf, DE; Uhde GmbH, 44141 Dortmund, DE 2004.
[13] S. Nakamura, T. Yasui, J. Catal. 17 (1970) 366–374.
[14] S. Nakamura, T. Yasui, J. Catal. 23 (1971) 315–320.
[15] Y.-F. Han, D. Kumar, C. Sivadinarayana, A. Clearfield, D.W. Goodman, Catal. Lett. 94 (2004) 131–134.
[16] M.S. Chen, D. Kumar, C.-W. Yi, D.W. Goodman, Science 310 (2005) 291–293.
[17] F. Calaza, Z. Li, F. Gao, J. Boscoboinik, W.T. Tysoe, Surf. Sci. 602 (2008) 3523–3530.
[18] W.D. Provine, P.L. Mills, J.J. Lerou, in: J.W. Hightower, W.N. Delgass, E. Iglesia, A.T. Bell (Eds.), 11th International Congress on Catalysis, Elsevier, 1996, pp. 191–200.
[19] K. Luo, T. Wei, C.-W. Yi, S. Axnanda, D.W. Goodman, J. Phys. Chem. B 109 (2005) 23517–23522.
[20] Y. Xiang, X. Wu, D. Liu, X. Jiang, W. Chu, Z. Li, Y. Ma, W. Zhou, S. Xie, Nano Lett. 6 (2006) 2290–2294.
[21] S.J. Mejía-Rosales, C. Fernández-Navarro, E. Pérez-Tijerina, D.A. Blom, L.F. Allard, M. José-Yacamán, J. Phys. Chem. C 111 (2007) 1256–1260.
[22] N. Toshima, T. Yonezawa, New J. Chem. 22 (1998) 1179–1201.
[23] Y. Mizukoshi, T. Fujimoto, Y. Nagata, R. Oshima, Y. Maeda, J. Phys. Chem. B 104 (2000) 6028–6032.
[24] R.W.J. Scott, O.M. Wilson, R.M. Crooks, J. Phys. Chem. B 109 (2005) 692–704.
[25] S. Chandra, S. Dietrich, H. Lang, D. Bahadur, J. Mater. Chem. 21 (2011) 5729–5737.
[26] S. Dietrich, S. Schulze, M. Hietschold, H. Lang, J. Colloid Interface Sci. 359 (2011) 454–460.
[27] S. Dietrich, S. Chandra, C. Georgi, S. Thomas, D. Makarov, S. Schulze, M. Hietschold, M. Albrecht, D. Bahadur, H. Lang, Mater. Chem. Phys. 132 (2012) 292–299.
[28] Y. Niu, R.M. Crooks, C. R. Chim. 6 (2003) 1049–1059.
[29] E. Boisselier, A.K. Diallo, L. Salmon, C. Ornelas, J. Ruiz, D. Astruc, J. Am. Chem. Soc. 132 (2010) 2729–2742.
[30] J.A. Creighton, D.G. Eadont, J. Chem. Soc. Faraday Trans. 87 (1991) 3881–3891.
[31] M.-L. Wu, D.-H. Chen, T.-C. Huang, Langmuir 17 (2001) 3877–3883.
[32] N. Toshima, M. Harada, Y. Yamazaki, K. Asakura, J. Phys. Chem. 96 (1992) 9927–9933.
[33] M.-M. Pohl, J. Radnik, M. Schneider, U. Bentrup, D. Linke, A. Brückner, E. Ferguson, J. Catal. 262 (2009) 314–323.
[34] A. Baylet, P. Marécot, D. Duprez, P. Castellazzi, G. Groppi, P. Forzatti, Phys. Chem. Chem. Phys. 13 (2011) 4607–4613.
[35] K.-T. Park, D.L. Novikov, V.A. Gubanov, A.J. Freeman, Phys. Rev. B 49 (1994) 4425–4431.